Scintillation and spectroscopy of the pure and Ce^{3+}-doped elpasolites: Cs_2LiYX_6 (X = Cl, Br)

2002 J. Phys.: Condens. Matter 14 8481

(http://iopscience.iop.org/0953-8984/14/36/307)

INSTITUTE OF PHYSICS PUBLISHING JOURNAL OF PHYSICS: CONDENSED MATTER

J. Phys.: Condens. Matter **14** (2002) 8481–8496 PII: S0953-8984(02)36536-6

Scintillation and spectroscopy of the pure and Ce^{3+}-doped elpasolites: Cs_2LiYX_6 (X = Cl, Br)

E V D van Loef[1], P Dorenbos[1,3], C W E van Eijk[1], K W Krämer[2] and H U Güdel[2]

[1] Radiation Technology Group, Interfaculty Reactor Institute, Delft University of Technology, Mekelweg 15, 2629 JB Delft, The Netherlands
[2] Department of Chemistry and Biochemistry, University of Bern, Freiestrasse 3, 3000 Bern 9, Switzerland

E-mail: dorenbos@iri.tudelft.nl

Received 2 May 2002
Published 29 August 2002
Online at stacks.iop.org/JPhysCM/14/8481

Abstract

The optical and scintillation properties of pure and Ce^{3+}-doped Cs_2LiYX_6 (X = Cl, Br) are presented. X-ray-excited optical luminescence spectra, optical excitation and emission spectra, time-resolved excitation and emission spectra, scintillation pulse height spectra and scintillation decay time spectra of Ce^{3+}-doped Cs_2LiYX_6 (X = Cl, Br) crystals measured from 10 to 300 K are presented. Factors influencing the scintillation mechanism and the presence of core–valence luminescence are discussed.

1. Introduction

Since the discovery of the scintillator NaI(Tl) by Hofstadter [1, 2] significant progress has been made in the research and development of inorganic scintillators for the detection of ionizing radiation. Basically, two different directions have been pursued during the five decades of scintillator research:

(1) the search and development of new inorganic scintillators dedicated to specific applications and
(2) the optimization of scintillators, like $PbWO_4$ [3, 4] BGO [5, 6] NaI(Tl) [7–9] and CsI(Tl) [7, 8, 10–12].

However, both directions have largely been fields of trial and error. High density, stability in air and ease of crystal growth were the main criteria which led to the discovery of most of the scintillators used nowadays. In general, attention was focused on the characterization of the scintillation properties, and theoretical work on scintillators is scarce. Only a few studies present a more detailed investigation of the scintillation mechanism [13–19]. Nevertheless,

[3] Author to whom any correspondence should be addressed.

many inorganic materials were found to be efficient scintillators with a high light yield and good energy resolution. Unfortunately, the question why these materials showed such excellent scintillation properties remained open, due to the lack of in-depth knowledge about the scintillation mechanism.

In order to gain more insight into the scintillation mechanism we studied the pure and Ce^{3+}-doped elpasolites: Cs_2LiYX_6:Ce^{3+} (with X = Cl, Br). Elpasolites with structural composition A_2BMX_6 (where A = Rb, Cs; B = Li, Na, K; M = Y, La–Lu and X = F, Cl, Br, I) are model systems investigated in numerous optical, scintillation and magnetic studies. They have the advantage over many other crystalline systems that the M^{3+} site, located at the centre of a regular octahedron of halide ions X^-, offers a natural environment for the incorporation of Ce^{3+} and other trivalent ions. The fact that the crystal structure of Cs_2LiYX_6 remains the same for X = Cl and Br enables us to study the effect of the anion on the scintillation mechanism in particular.

In this work we present a short review of models for scintillation mechanisms in inorganic scintillators. We review the existing data on the optical and scintillation properties and, in particular, the scintillation mechanism of chloro- and bromo-elpasolites. We present new data on pure and Ce-doped Cs_2LiYX_6 (X = Cl, Br) and finally the scintillation mechanism in these materials is discussed.

2. Scintillation mechanisms

2.1. Models on scintillation mechanisms

When discussing scintillation mechanisms, it is useful to make a distinction between the *scintillation process* and the *scintillation mechanism*. Here we define the *scintillation process* as the consecutive stages of

(a) interaction of radiation with matter, creation of primary electrons and the relaxation and thermalization of the electrons and holes,
(b) the formation of electron–hole pairs and energy transfer to a luminescent centre and
(c) luminescence.

In contrast, the *scintillation mechanism* is the method by which the energy is transferred by the electron–hole pairs to the luminescent centre. Obviously, we can only speak about the *scintillation mechanism* if we consider impurity-activated inorganic scintillator materials. For intrinsically pure materials, light is produced by recombination of the electrons and holes and energy transfer as such does not occur.

Various models have been used to describe each of these three stages of the scintillation process, but only for (a) and (c) are workable theoretical models available. Nevertheless, different models of energy transfer have been presented in the past, based on the assumption that energy transfer was dependent on energy carrier density and electron stopping power [13, 14]. Both are material specific properties that can be simulated using dedicated Monte Carlo codes.

In the following discussion, we distinguish two categories of inorganic scintillators as a matter of convenience: intrinsically pure inorganic scintillators, like BaF_2 and BGO, and impurity-activated inorganic scintillators, like NaI(Tl), CsI(Tl) and $LaCl_3$(Ce). Since our objective is to discuss the *scintillation mechanism*, our focus will be on impurity-activated inorganic scintillators, in particular on Ce^{3+}-activated materials. In general we can define three different *scintillation mechanisms* corresponding to three different *energy transfer mechanisms* which occur at different timescales and with different probabilities.

(i) *Energy transfer by direct electron–hole capture.* This type of energy transfer is desired for impurity-(Ce^{3+}-) activated inorganic scintillator materials. After absorbing a γ-ray quantum, free electrons and holes are created in the conduction band and valence band, respectively. These free electron and holes may be trapped within 1 ns by a Ce^{3+} ion and the observed decay time is characteristic of the lifetime of the excited state of Ce^{3+}.

(ii) *Energy transfer by binary electron–hole recombination.* Instead of being trapped by Ce^{3+}, the hole can also be trapped by the host forming a V_k or H centre within a few picoseconds. Next, the mobile V_k or H centre can be trapped by a Ce^{3+} ion. Recombination with the electron will eventually excite the Ce^{3+} centre. Alternatively, it is also possible that Ce^{3+} traps the electron first, and that the V_k or H centre diffuses to Ce^{3+}. If one assumes
   (a) such a kind of binary electron–hole recombination,
   (b) that the electrons and holes are distributed randomly and
   (c) that the electron diffusion migration is random, theoretically the decay is described by a $(1 + at)^{-2}$ dependence [20].

(iii) *Energy transfer by STE diffusion/emission.* After the creation of electrons and holes, the hole may form a V_k centre. If this self-trapped hole binds a free electron, a self-trapped exciton (STE) is formed. Also, STEs may be created directly during the relaxation of free electron–hole pairs.

The STE can transfer its energy to the activator by two different mechanisms, i.e. (non-) radiative energy transfer, or STE diffusion. In the first case, overlap between the STE emission and the energy levels of the activator ion (Ce^{3+}) is necessary. For this type of energy transfer a strong temperature dependence is not expected and the scintillation decay associated with this mechanism is characteristic of the lifetime of the STE.

In the second case, the diffusion process is thermally activated and the mobility of the STE increases when the temperature rises. However, STE emission is usually thermally quenched at elevated temperatures and thus there will be an optimum temperature for maximum transport efficiency. The latter mechanism can be described by a set of two coupled differential equations that predict an anti-correlation between luminescence yields of STE and Ce^{3+}. Accordingly, a scintillation decay is expected that is determined by the lifetime of the STE and the rate of energy transfer from the STE to Ce^{3+}.

2.2. Scintillation mechanisms in the elpasolites

The chloro- and bromo-elpasolites with composition A_2BMX_6 (with A = Rb, Cs; B = Li, Na, K; M = La–Lu; X = Cl, Br) are attractive materials to study d–f transitions in rare-earth ions due to the presence of a trivalent cationic site with perfect O_h symmetry. Additionally, the Li-containing elpasolites are possible candidates for neutron sensitive scintillators, as Li-containing compounds possess the ability to convert incident neutrons into secondary ionizing particles by the reaction (1)

$$^{6}_{3}\mathrm{Li} + ^{1}_{0}\mathrm{n} \rightarrow ^{3}_{1}\mathrm{H} + \alpha. \tag{1}$$

These materials are of particular interest because of the possible presence of core–valence (CV) luminescence [21]. CV luminescence requires the creation of holes in a metal band by excitation of electrons from this band to the conduction band. Those holes are short lived and may recombine with electrons from the valence band. If this process proceeds radiatively it is called CV luminescence. By pulse shape discrimination techniques incident neutrons or alpha-particles can be distinguished from gamma-rays.

CV luminescence was observed for the first time in BaF_2 by Ershov *et al* [22] and studied in the chloro-elpasolite $Cs_2NaLaCl_6$ by Voloshinovskii *et al* [23]. The scintillation properties

of Cs_2NaMCl_6 (M = La, Ce, Lu) were studied by van't Spijker *et al* [24]. Unfortunately no CV luminescence was observed, probably because of absorption by impurity Ce^{3+}. Just recently, Ce^{3+}-doped $Cs_2LiLaCl_6$ was investigated by Rodnyi *et al* [25]. This compound shows CV luminescence, but no detailed study of the scintillation mechanism was reported. Combes *et al* investigated pure and Ce^{3+}-doped Cs_2LiYCl_6 [26] and reported for the first time on the scintillation mechanism in elpasolites. It was suggested that for low Ce concentrations, both radiative energy transfer from the STE to Ce^{3+} as well as STE diffusion to Ce^{3+} centres play an important role. For relatively high Ce concentrations, not the diffusion of the STE to Ce^{3+} centres appeared to be dominant, but trapping and stabilization of a V_k centre near Ce^{3+}. Electron paramagnetic resonance (EPR) studies on Cs_2NaYCl_6 by Pawlik and Spaeth [27] revealed that the V_k centre (Cl_2^-) is thermally stable up to liquid nitrogen temperatures. At lower temperatures, x-ray irradiation produces an intrinsic electron-trapping centre that was identified as a Jahn–Teller-distorted Y^{2+} defect. In the proper orientation, the V_k centre can couple to the intrinsic electron centre and form a Y^{2+}–V_k pair, which is regarded as an impurity-trapped STE. The recombination of the pair leads to STE luminescence. With respect to the bromo-elpasolites, a brief report on the scintillation properties of Ce^{3+}-doped Cs_2LiYBr_6 was published by Mishin *et al* [28].

3. Experimental techniques

3.1. Crystal growth

Cs_2LiYCl_6, Cs_2LiYCl_6:0.5% Ce^{3+}, Cs_2LiYBr_6 and Cs_2LiYBr_6:1% Ce^{3+} single crystals were grown by the vertical Bridgman technique in silica ampoules under vacuum. The starting materials were prepared from CsCl/Br (Merck, 99.9%), Li_2CO_3 (Heraeus, 99.995%), Y_2O_3 (Johnson and Matthey, 99.999%) and CeO_2 (Johnson and Matthey, 99.99%) according to the ammonium halide method [29, 30]. The crystals are hygroscopic and were sealed under helium atmosphere into small quartz ampoules to prevent hydration of the surfaces. The density of Cs_2LiYCl_6 and Cs_2LiYBr_6 is 3.31 and 4.15 g cm^{-3}, respectively.

3.2. Equipment

X-ray-excited optical luminescence spectra were recorded using an x-ray tube with a Cu anode operated at 35 kV and 25 mA. The emission was dispersed with an ARC VM504 monochromator (blazed at 300 nm, 1200 grooves mm^{-1}) and measured with an EMI 9462 photo-multiplier tube (PMT). The data are corrected for the wavelength dependence of the PMT quantum efficiency and the monochromator transmission.

High resolution, time-resolved excitation and emission spectra were recorded using synchrotron radiation at the SUPERLUMI station of the Synchrotron Strahlungslabor (HASYLAB) at the Deutsches Elektronen Synchrotron (DESY) in Hamburg, Germany. Emission spectra were recorded with an ARC Spectropro 300I monochromator (blazed at 300 nm, 300 grooves mm^{-1}) and a R6358 Hamamatsu PMT. Photons were counted within a time window of 13 ns following the start of the exciting synchrotron pulse. Another 81 ns wide time window starting 80 ns after the exciting pulse was used to discriminate between fast and slow luminescence components. Also the integral count rate was recorded. Excitation spectra were measured on a 2 m normal-incidence McPherson monochromator equipped with two interchangeable holographic gratings (1200 grooves mm^{-1}, blazed at 150 and 300 nm respectively). The wavelength accuracy was 0.3 nm. A description of both the SUPERLUMI station and the synchrotron operation characteristics is published in [31]. Excitation and emission spectra are corrected for the transmission of the system.

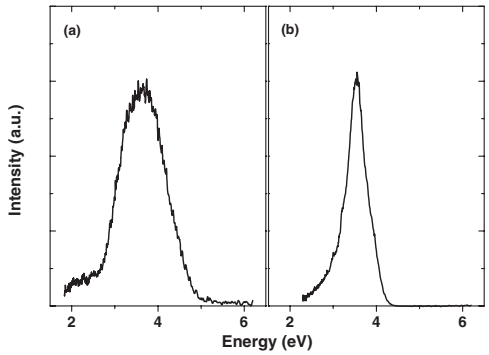

Figure 1. X-ray-excited optical luminescence spectra of (a) Cs_2LiYCl_6 and (b) Cs_2LiYBr_6 at 100 K.

Pulse-height spectra under excitation of γ-rays from a ^{137}Cs source were recorded with a Hamamatsu R1791 PMT with a box type dynode structure. It was connected to a homemade preamplifier and an Ortec 672 spectroscopic amplifier. The quartz ampoules containing the crystals were optically coupled onto the window of the PMT with Viscasil 60 000 cSt from General Electric. To minimize the light losses, the quartz ampoules were covered with several layers of 0.1 mm UV reflecting Teflon tape.

Scintillation decay times under ^{137}Cs 662 keV γ-ray excitation were recorded with a Philips XP2020Q PMT connected to a Tektronix TAS 380 oscilloscope or using standard start–stop techniques as described by Moses [32]. Scintillation decay time spectra under x-ray excitation were obtained from a pulsed x-ray excitation source [33] (pulse FWHM $\approx$1 ns) operated with an anode voltage of 35 kV_p and a pulse frequency of 100 kHz.

Decay time spectra as functions of temperature were recorded using an IBH Consultants Ltd hydrogen coaxial flashlamp (pulse FWHM $\approx$1 ns), an ARC VM504 monochromator (blazed at 300 nm, 1200 grooves mm^{-1}) and a Hamamatsu R943-02 PMT.

4. Results

4.1. X-ray-excited optical luminescence

X-ray-excited optical luminescence spectra of pure Cs_2LiYCl_6 [26] and Cs_2LiYBr_6 at 100 K are shown in figure 1. Cs_2LiYCl_6 emits in a broad band, centred at 3.6 eV (FWHM = 1.1 eV). Additionally, a low intensity emission occurs between 2 and 3 eV. Both bands are probably due to STE luminescence. For several other elpasolites [24] and bromides [34, 35] similar bands have been observed in this spectral range and were readily ascribed to STE luminescence. In the case of Cs_2LiYBr_6, the emission spectrum is dominated by a single broad band at 3.6 eV (FWHM = 0.6 eV). The emission deviates from a Gaussian band shape, which is expected for a linear coupling to one dominant vibrational mode. At this time it is not clear whether the low energy tail is due to an additional, weak emission band, or a second-order electron–lattice coupling.

Figure 2 shows the x-ray-excited optical luminescence spectra of Cs_2LiYCl_6:Ce^{3+} [26] and Cs_2LiYBr_6:Ce^{3+} [28] recorded at room temperature. The chloride spectrum (solid trace) is dominated by the characteristic doublet of the $5d \rightarrow 4f$ Ce^{3+} luminescence with maxima at 3.1 and 3.3 eV. The transitions from the lowest $5d^1$ excited state to the $^2F_{5/2}$ ground state and the $^2F_{7/2}$ state of the $4f^1$ configuration are nicely resolved. The spin–orbit splitting between

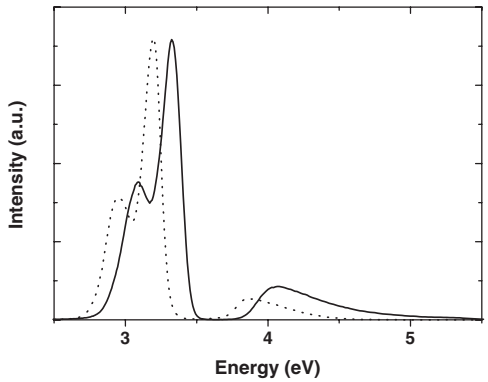

Figure 2. X-ray-excited optical luminescence spectra of $Cs_2LiYCl_6:Ce^{3+}$ (solid trace) and $Cs_2LiYBr_6:Ce^{3+}$ (dotted trace) at room temperature.

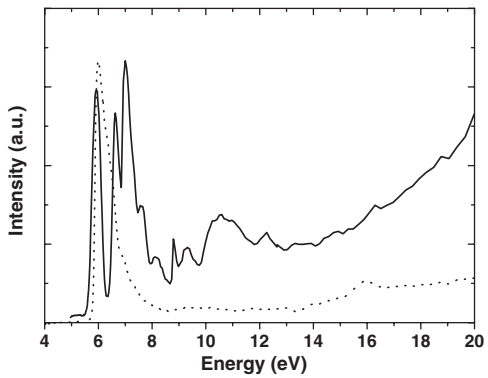

Figure 3. Optical excitation spectra of Cs_2LiYCl_6 (solid trace) and Cs_2LiYBr_6 (dotted trace) at 10 K monitoring the host lattice emission at 3.6 eV.

the ^2F states is ∼0.2 eV. The weak broad band around 4 eV is attributed to residual host lattice emission. The absence of luminescence between 3.5 and 3.8 eV is due to the absorption of host lattice emission by Ce^{3+}. For the bromide (dotted trace) the shape of the spectrum is very similar to that of the chloride. The luminescence maxima are observed at 3.0 and 3.2 eV. Again, the absence of luminescence between 3.3 and 3.6 eV is ascribed to the absorption of host lattice emission by Ce^{3+}.

4.2. Optical excitation and emission

The optical excitation spectra of pure Cs_2LiYCl_6 and Cs_2LiYBr_6 at 10 K monitoring the host lattice emission at 3.6 eV are depicted in figure 3. The excitation spectrum of Cs_2LiYCl_6 (solid trace) consists of a structured band with maxima at 5.9, 6.6 and 7.0 eV. A much weaker band is observed near 10.6 eV. The intensity of the excitation spectrum gradually increases above 14 eV. A single band at 6.0 eV dominates the excitation spectrum of Cs_2LiYBr_6. If the low energy side of this peak is taken as the onset of the valence-to-conduction band transition, then the bandgap of Cs_2LiYBr_6 is about 5.7 eV.

Figure 4 shows the 10 K emission spectra of (a) Cs_2LiYCl_6 excited at (i) 5.9 eV, (ii) 7.0 eV and (iii) 10.8 eV and (b) Cs_2LiYBr_6 excited at 6.0 eV. The emission spectrum of Cs_2LiYCl_6,

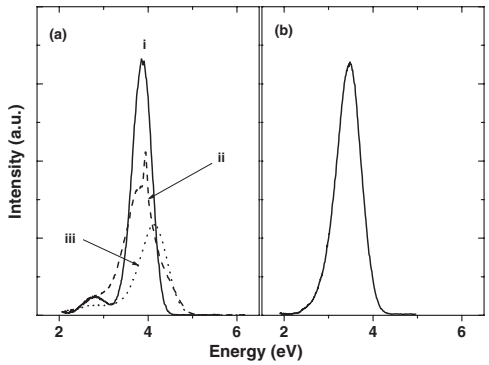

Figure 4. Optical emission spectra of (a) Cs_2LiYCl_6 excited at (i) 5.9 eV, (ii) 7.0 eV and (iii) 10.8 eV, and (b) Cs_2LiYBr_6 excited at 6.0 eV. All spectra were recorded at 10 K.

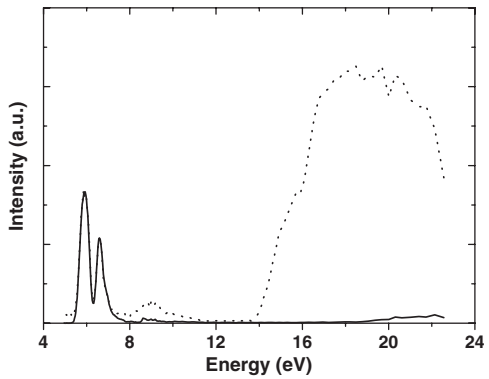

Figure 5. Time-resolved optical excitation spectra of Cs_2LiYCl_6 at 194 K monitoring the host lattice emission at 4.5 eV. The dotted curve represents the 13 ns gated excitation spectrum, whereas the solid curve represents the 81 ns gated excitation spectrum.

under 5.9 eV excitation, shows a band at 3.8 eV (FWHM = 0.4 V) which is attributed to STE luminescence. At lower energy, near 2.8 eV, an additional weaker band can be distinguished (FWHM = 0.7 eV). Excitation at 6.6 or 7.0 eV yields a broad emission band at 3.6 eV similar to that shown in figure 1(a). However, there is an additional sharp peak near 3.9 eV, which is probably due to $^6P_{7/2} \rightarrow {}^8S_{7/2}$ emission of a Gd^{3+} impurity. Excitation into the low intensity band near 10.6 eV gives rise to another emission at 4.1 eV (FWHM = 0.6 eV). The emission spectrum of Cs_2LiYBr_6 consists of a single band at 3.4 eV (FWHM = 0.6 eV).

Time-resolved excitation spectra of Cs_2LiYCl_6 at 194 K monitoring the host lattice emission at 4.5 eV are shown in figure 5. Between 14 and 24 eV an intense broad band is observed in the 13 ns gated excitation spectrum (dotted trace). This band is not present either in the 81 ns gated excitation spectrum (solid trace), or in the excitation spectra of the 3.6 and 4.1 eV emission bands (see figure 3). Apparently, the band corresponds to an excited state with a short lifetime, whereas excitation into the peaks at 5.9 and 6.6 eV leads to luminescence with a long decay time. A similar intense, broad excitation was observed by Rodnyi *et al* [25] for pure and Ce^{3+}-doped $Cs_2LiLaCl_6$. They ascribed it to an excitation of 5p Cs levels. The peak observed at 7.0 eV in the excitation spectrum of Cs_2LiYCl_6 monitoring host lattice emission at 3.6 eV (figure 3, solid trace) is not observed in the time-resolved excitation spectrum (figure 5).

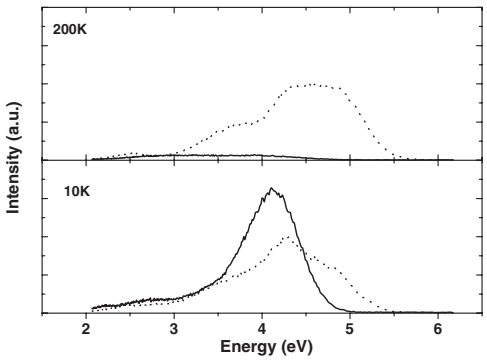

Figure 6. Time-resolved optical emission spectra of Cs_2LiYCl_6 at 10 and 200 K excited at 17.2 eV. The dotted curves represent the 13 ns gated emission spectra, whereas the solid curves represent the 81 ns gated emission spectra.

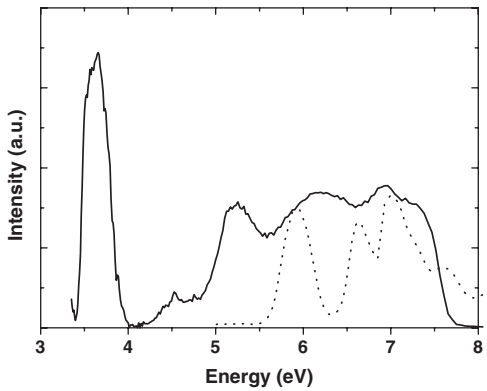

Figure 7. Excitation spectrum of Cs_2LiYCl_6:Ce^{3+} at 130 K monitoring the Ce^{3+} emission at 3.1 eV. The dotted trace represents the excitation spectrum of pure C_2LiYCl_6 at 10 K.

It seems that the two peaks at 5.9 and 6.6 eV have a different origin from the peak at 7.0 eV. The former two are probably due to direct excitation of STEs, whereas the latter is likely the onset of a band-to-band transition at 6.8 eV.

Time-resolved emission spectra of Cs_2LiYCl_6 excited at 17.2 eV are shown in figure 6 for 10 and 200 K. The 13 ns gated spectrum (dotted trace) at 200 K shows a broad structured band between 3 and 6 eV. It is probably composed of two different emissions with maxima near 3.7 and 4.5 eV. Those emissions are completely absent in the 81 ns gated emission spectrum (solid trace) and are ascribed to CV luminescence [25]. At 10 K, the intensity of the broad structured band decreases in favour of a 0.6 eV wide emission with a maximum near 4.1 eV. Its shape deviates from a Gaussian form. It is only present in the 81 ns gated spectra between 10 and 100 K and probably due to some type of STE luminescence.

Figure 7 shows the excitation spectrum of Cs_2LiYCl_6:Ce^{3+} [26] at 130 K monitoring the Ce^{3+} emission at 3.1 eV (solid curve). For comparison pure Cs_2LiYCl_6 (dotted curve) is shown as well. The Cs_2LiYCl_6:Ce^{3+} spectrum is dominated by the intense band of the $Ce^{3+}4f(^2F_{5/2}) \rightarrow 5d(t_{2g})$ transitions between 3.4 and 4.0 eV. Four further broad bands are observed near 4.5, 5.3, 6.2 and 6.9 eV. Excitation near 4.5 and 5.3 eV predominantly results in Ce^{3+} emission, whereas excitation around 6.2 and 6.9 eV yields both Ce^{3+} and STE emission.

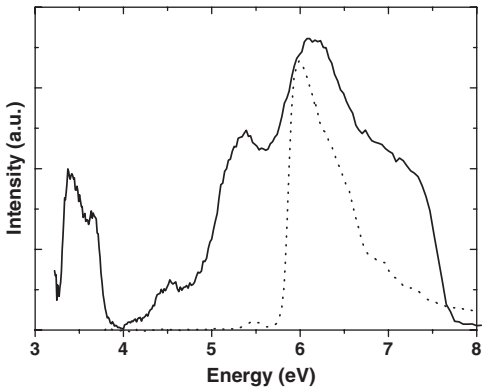

Figure 8. Excitation spectrum of Cs_2LiYBr_6:Ce^{3+} at 130 K monitoring the Ce^{3+} emission at 3.0 eV. The dotted trace represents the excitation spectrum of pure Cs_2LiYBr_6 at 10 K.

Since the bands near 4.5 and 5.3 eV are completely absent in the optical excitation spectrum of pure Cs_2LiYCl_6, they are both ascribed to Ce^{3+} transitions. That near 4.5 eV might be due to a Ce^{3+} centre of lower symmetry [28] caused for example by aggregation of Ce^{3+} ions. The band near 5.3 eV is ascribed to $Ce^{3+}4f(^2F_{5/2}) \rightarrow 5d(e_g)$ transitions. Accordingly, the $5d(t_{2g} - e_g)$ crystal field splitting is $\varepsilon_{cfs} = 15\,300 \pm 2400\ cm^{-1}$, which is relatively small compared to numbers for chloro-elpasolites reported by Dorenbos [36]. Nevertheless, it compares well with the results for $Cs_2NaLuCl_6$:Ce^{3+} [24] and $Cs_2LiLaCl_6$:Ce^{3+} [25]. The bands near 6.2 and 6.9 eV are due to direct STE excitation and band-to-band transitions, respectively. However, Cs_2LiYCl_6:Ce^{3+} is also efficiently excited in the region between 5.3 and 6.2 eV. Possibly, it is due to the increase in temperature which broadens the excitation bands considerably, but it can also be due to $Ce^{3+}4f \rightarrow 6s$ transitions. At the moment we cannot discriminate between the two.

The excitation spectrum of Cs_2LiYBr_6:Ce^{3+} at 130 K monitoring the Ce^{3+} emission at 3.0 eV is shown in figure 8 (solid trace). The $Ce^{3+}4f \rightarrow 5d(t_{2g})$ transitions of the bromide are found at lower energies than for the chloride, i.e. between 3.2 and 3.9 eV. The $Ce^{3+}4f \rightarrow 5d(e_g)$ transition is located at 5.3 eV which results in a $5d(t_{2g} - e_g)$ crystal field splitting of $\varepsilon_{cfs} = 17\,300 \pm 1300\ cm^{-1}$. Similar values for the energy and the 5d crystal field splitting of Ce^{3+} have been reported for other bromides [34]. It is remarkable that for Cs_2LiYCl_6:Ce^{3+} the $Ce^{3+}4f \rightarrow 5d(t_{2g})$ transitions are more intense than the band-to-band transitions between 6 and 7 eV, whereas it is the other way around for the bromide.

4.3. Light yield

The scintillation pulse height spectrum of Cs_2LiYBr_6:Ce^{3+} at room temperature excited with 662 keV γ-rays from a ^{137}Cs source using a shaping time of 10 μs is shown in figure 9. The photopeak at 662 keV and the Compton edge near 450 keV are clearly visible. The sharp peak at 32 keV is caused by Ba x-rays emitted from the source. The energy resolution of the photopeak is $9 \pm 1\%$. The light yield amounts to $25\,000 \pm 5000$ photons per MeV (ph MeV^{-1}) of absorbed γ-ray energy. The results for the different compounds under investigation are summarized in table 1.

The temperature dependence of the relative light yield under x-ray excitation is shown for pure Cs_2LiYCl_6 (solid trace) and Cs_2LiYBr_6 (dotted trace) in figure 10. For both compounds the light yield decreases with temperature due to the quenching of STE luminescence.

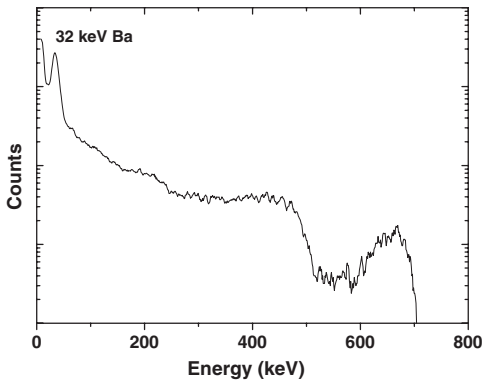

Figure 9. Pulse height spectrum of $Cs_2LiYBr_6:Ce^{3+}$ at room temperature excited with 662 keV gamma rays from a ^{137}Cs source using a shaping time of 10 μs.

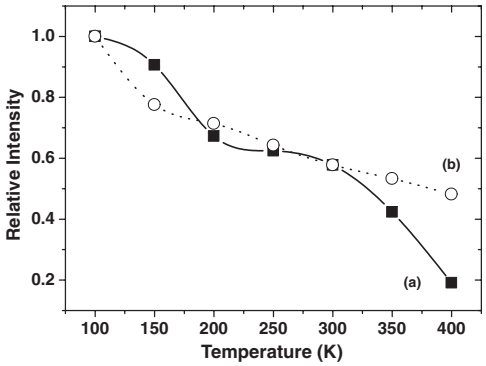

Figure 10. Temperature dependence of the light yield of (a) Cs_2LiYCl_6 and (b) Cs_2LiYBr_6 under x-ray excitation. The curves are a guide to the eye.

Table 1. Light yield and energy resolution of Cs_2LiYCl_6, $Cs_2LiYCl_6:Ce^{3+}$, Cs_2LiYBr_6 and $Cs_2LiYBr_6:Ce^{3+}$. The data for Cs_2LiYCl_6 and $Cs_2LiYCl_6:Ce^{3+}$ have been taken from [26].

	Light yield (10^3 ph MeV^{-1})			
Compound	1 μs	10 μs	Energy resolution R (%, 10 μs)	Reference
Cs_2LiYCl_6	7 ± 1	22 ± 2	11 ± 1	[26]
Cs_2LiYCl_6:0.5 Ce^{3+}	10 ± 1	18 ± 2	7 ± 1	[26]
Cs_2LiYBr_6	12 ± 1	24 ± 2	11 ± 1	
Cs_2LiYBr_6:1% Ce^{3+}	17 ± 2	25 ± 3	9 ± 1	

Figure 11 shows the behaviour of the Ce^{3+}-doped compounds $Cs_2LiYCl_6:Ce^{3+}$ (solid trace) and $Cs_2LiYBr_6:Ce^{3+}$ (dotted trace) which is distinctly different from that of the pure ones. Both traces show a maximum at 300 and 200 K for the chloride and bromide, respectively.

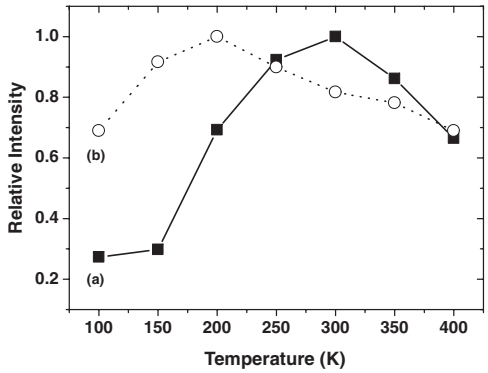

Figure 11. Temperature dependence of the light yield of (a) $Cs_2LiYCl_6:Ce^{3+}$ and (b) $Cs_2LiYBr_6:Ce^{3+}$ under x-ray excitation. The curves are a guide to the eye.

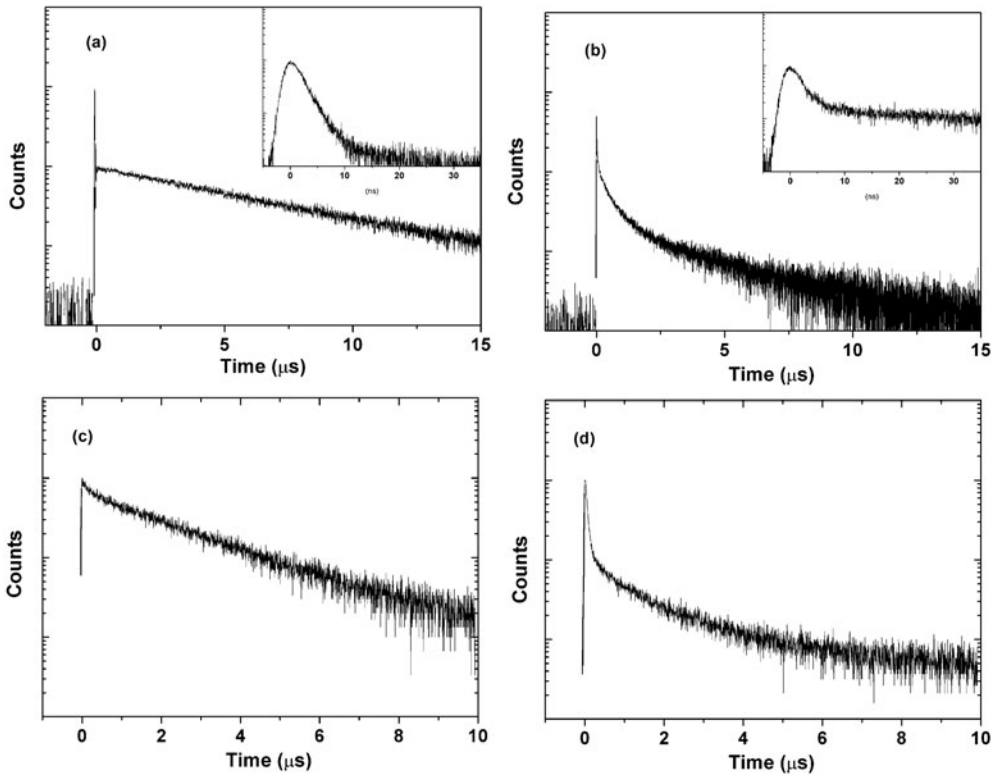

Figure 12. Scintillation decay time spectra of (a) Cs_2LiYCl_6, (b) $Cs_2LiYCl_6:Ce^{3+}$, (c) Cs_2LiYBr_6 and (d) $Cs_2LiYBr_6:Ce^{3+}$ at room temperature under ^{137}Cs γ-ray excitation.

4.4. Scintillation decay

Figure 12 shows the scintillation decay time spectra of (a) Cs_2LiYCl_6, (b) $Cs_2LiYCl_6:Ce^{3+}$, (c) Cs_2LiYBr_6 and (d) $Cs_2LiYBr_6:Ce^{3+}$ at room temperature under ^{137}Cs γ-ray excitation. The insets in figures 12(a) and (b) show the decay time spectra under pulsed x-ray excitation on a shorter timescale for Cs_2LiYCl_6 and $Cs_2LiYCl_6:Ce^{3+}$, respectively. The decay curve

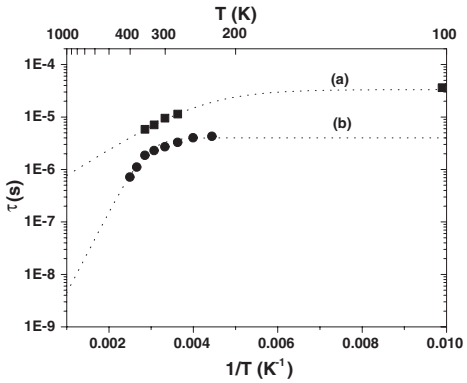

Figure 13. Decay time of the STE, τ, in (a) Cs_2LiYCl_6 and (b) Cs_2LiYBr_6 as a function of temperature.

Table 2. The activation energy for thermal decay, ΔE, the lifetime of radiative decay, τ_R, and thermal decay, τ_t, for STEs in Cs_2LiYCl_6 and Cs_2LiYBr_6.

Compound	ΔE (eV)	τ_t (ps)	τ_R (μs)
Cs_2LiYCl_6	0.10 ± 0.01	—	33 ± 5
Cs_2LiYBr_6	0.30 ± 0.03	150 ± 50	4 ± 1

of Cs_2LiYCl_6 is characterized by two components: a fast one with a lifetime of 2 ± 1 ns, characteristic for CV luminescence in Cs-based chlorides [37, 38], and a slow component with a decay time of 6.9 ± 0.1 μs due to STE luminescence. Both components are also present in the Cs_2LiYCl_6:Ce^{3+} spectra but the slow component has a shorter lifetime of 4.3 ± 0.1 μs probably due to both STE and Ce^{3+} luminescence. However, there are further contributions that can be modelled by a non-exponential decay with a lifetime of about 400 ns. The only compound that seems to have a single-exponential decay is Cs_2LiYBr_6. Its luminescence has a lifetime of 2.4 ± 0.2 μs. The decay curve of Cs_2LiYBr_6:Ce^{3+} can be described by three decay components: a relatively fast component of 65 ± 5 ns, typical for Ce^{3+} luminescence, an intermediate, non-exponential one of 1.1 ± 0.1 μs and a slow one of 9 ± 1 μs. The latter are probably due to Ce^{3+} and STE luminescence, respectively. Neither bromide shows a fast component due to CV luminescence.

In figure 13 the decay time τ of the STE in (a) Cs_2LiYCl_6 and (b) Cs_2LiYBr_6 is presented as a function of $1/T$. The samples were excited at 5.9 and 6.0 eV respectively, monitoring all host lattice emissions. The dotted curves show model calculations according to

$$\frac{1}{\tau} = \frac{1}{\tau_R} + \frac{1}{\tau_t} \exp\left(-\frac{\Delta E}{kT}\right). \tag{2}$$

$1/\tau_R$ and $(1/\tau_t)\exp(-\Delta E/kT)$ are the probabilities of radiative and thermal decay, respectively, ΔE is the activation energy for thermal decay and k the Boltzmann constant. From a fit to equation (2) values for ΔE, τ_R and τ_t were obtained. They are summarized in table 2. The activation energies for thermal decay ΔE are 100 ± 10 and 300 ± 30 meV, for Cs_2LiYCl_6 and Cs_2LiYBr_6 respectively. The lifetime of radiative decay, τ_R, of the STE in Cs_2LiYBr_6 is significantly shorter than in Cs_2LiYCl_6.

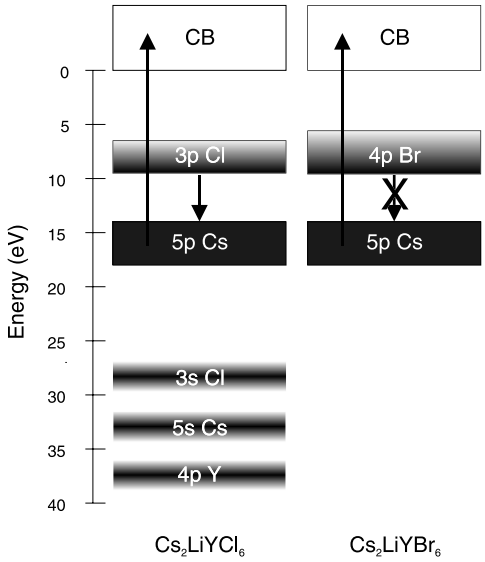

Figure 14. Energy band scheme of Cs_2LiYCl_6 and Cs_2LiYBr_6. The large arrow represents the 5p Cs core excitation, whereas the smaller arrow represents CV luminescence. In the case of Cs_2LiYBr_6 no CV luminescence was observed.

5. Discussion

Pure Cs_2LiYCl_6 shows a broad structured emission band between 3 and 6 eV (see figure 6), with a fast decay time ($\tau \approx 10^{-9}$ s) due to CV luminescence. A model for CV transitions, according to which the energy position and width of the CV luminescence bands depend on the position and width of the 3p Cl valence band and the 5p Cs core band, can be used to rationalize the situation in the band structure picture shown in figure 14. The energies of the bands were calculated using the GAUSSIAN98 (G98) program [39]. The widths of the 3p Cl and 5p Cs bands were taken to be 3 and 4 eV [23], respectively, and the bandgap energy $E_g = 6.8$ eV (see figure 3). In contrast to the chloride Cs_2LiYBr_6 does not show CV luminescence. Apparently, the condition for the detection of CV band transitions [21] is not met in Cs_2LiYBr_6, probably because of the relatively high probability of the competing Auger decay. The latter assumption is supported by the fact that the bandgap of Cs_2LiYBr_6 is smaller than for Cs_2LiYCl_6, 5.7 and 6.8 eV, respectively. Hence, CV luminescence is more easily quenched in Cs_2LiYBr_6 than in Cs_2LiYCl_6 (see figure 14).

Unfortunately, the contribution of CV luminescence to the total light yield is relatively small in Cs_2LiYCl_6. The major contribution to the total light yield is recombination luminescence from STEs. In both Cs_2LiYCl_6 and Cs_2LiYBr_6, STE luminescence is observed with a long lifetime of the order of 1–10 μs and a large activation energy for thermal decay of the order of 100–300 meV. For most alkaline-earth halides [40] and for KI [41, 42], an equally large activation energy for thermal decay was reported, but most other alkali halides [43] show STE luminescence with a decay time and activation energy for thermal decay being an order of magnitude lower. Although the energy of the STE luminescence band overlaps with $Ce^{3+}4f \rightarrow 5d$ transitions, in both Cs_2LiYCl_6:Ce^{3+} and Cs_2LiYBr_6:Ce^{3+} (compare figure 1 with 6), there is still some STE luminescence present in the room temperature x-ray excited optical luminescence spectra of Cs_2LiYCl_6:Ce^{3+} and Cs_2LiYBr_6:Ce^{3+} (see figure 2).

Apparently, energy transfer from the STE to Ce^{3+} centres is somehow inefficient and occurs to a large extent radiatively. Radiative energy transfer due to absorption of STE luminescence by Ce^{3+} ions results in Ce^{3+} emission and a dip in the STE emission band at the position of the Ce^{3+} absorption band (see figure 2). In this case, the effective lifetime of the Ce^{3+} emission equals the lifetime of the STE. It is expected that for this type of energy transfer the luminescence intensity as a function of temperature decreases with increasing temperature due to the quenching of STE luminescence.

One needs an additional mechanism acting in parallel to explain the bell-shaped curves shown in figure 11. That is, one needs to explain the *increase* in the relative light yield, from 100 to 300 K and from 100 to 200 K for Cs_2LiYCl_6:Ce^{3+} and Cs_2LiYBr_6:Ce^{3+}, respectively, and subsequently the *decrease* in the relative light yield for both Cs_2LiYCl_6:Ce^{3+} and Cs_2LiYBr_6:Ce^{3+} up to 400 K.

An additional mechanism acting in parallel could be non-radiative energy transfer from STE to Ce^{3+}, i.e. *STE diffusion*, or *binary electron–hole recombination* on Ce^{3+}. In the first case, the transfer rate increases with mobility, i.e. temperature, resulting in an increase in Ce^{3+} luminescence at the expense of STE luminescence [19]. Consequently, the effective lifetime of the STE decreases. As can be observed in figures 12(b) and (d) versus (a) and (c), the slow decay component, i.e. a mix of STE and Ce^{3+} luminescence for the Ce-doped compounds, has decreased. *Binary electron–hole recombination* on Ce^{3+} could explain the non-exponential decay component in the decay curves of Cs_2LiYCl_6:Ce^{3+} and Cs_2LiYBr_6:Ce^{3+}. In principle, it is possible that after the creation of a STE, the bound electron and hole separate again and form an F–H or F–V_k pair [44]. This process is thermally activated and one expects an increase in loosely bound electrons (F centres) and holes (H or V_k centres) with increasing temperature. Next, the V_k centre is trapped or stabilized near a Ce^{3+} ion and recombination with the electron will eventually excite the Ce^{3+} centre. Alternatively, it is possible that the electron is trapped or stabilized in the vicinity of a Ce^{3+} ion and subsequently the hole recombines with the (Ce^{3+}–e^-) species to yield Ce^{3+} luminescence. Unfortunately, we cannot discriminate between the two alternatives, although we think that *STE diffusion* plays a minor role in the scintillation mechanism. The fact that the contribution of the fast decay component due to direct capture of electrons and holes by Ce^{3+} is virtually absent or relatively small in Cs_2LiYCl_6:Ce^{3+} and Cs_2LiYBr_6:Ce^{3+}, respectively, indicates that trapping of electrons and holes by Ce^{3+} does not occur on a large scale in these materials. The majority of the free electrons and holes form either an intrinsic or impurity- (Ce^{3+}-) perturbed STE which is relatively stable in pure and Ce^{3+}-doped Cs_2LiYCl_6 and Cs_2LiYBr_6.

The main difference between Cs_2LiYCl_6 and Cs_2LiYBr_6 is found in the lifetime of radiative decay of the STE. In Cs_2LiYBr_6 ($\tau_R \approx 3\ \mu s$) it is smaller than in Cs_2LiYCl_6 ($\tau_R \approx 33\ \mu s$) due to the stronger spin–orbit coupling of the ground state [45] of the STE in Cs_2LiYBr_6. Additionally, the spin–orbit splitting of the halogen p valence bands increases as the halogen atom becomes heavier [46]. Since both Cs_2LiYCl_6 and Cs_2LiYBr_6 have exactly the same crystal structure, the valence band in Cs_2LiYBr_6 is broader than the valence band in Cs_2LiYCl_6. Consequently, free holes will move more easily through the valence band in the case of Cs_2LiYBr_6. Assuming that in both cases free electrons move faster than free holes, fast Ce^{3+} luminescence is observed if the diffusion rate of the holes is of the order of magnitude of the time needed to create a STE. Since this process is dependent on the Ce concentration, it is expected that increasing the Ce concentration will lead to an increase in the contribution of the short decay component to the total light yield.

Acknowledgments

These investigations are supported by the Netherlands Technology Foundation (STW), the IHP contract HPRI-CT-1999-00040 of the European Commission and by the Swiss National Science Foundation. The authors thank Dr M Kirm for his assistance in the SUPERLUMI experiments at the HASYLAB of DESY, Hamburg, and P A Rodnyi for supplying some of the data in figures 11(a) and (b).

References

[1] Hofstadter R 1948 *Phys. Rev.* **74** 100
[2] Hofstadter R 1949 *Phys. Rev.* **75** 796
[3] Lecoq P 1997 *Proc. SCINT 97* ed Yin Zhiwen, Li Peijun, Fen Xiqi and Xue Zhilim (Shanghai, China: CAS Shanghai Branch Press) p 13
[4] Kobayashi M *et al* 1997 *Proc. SCINT 97* ed Yin Zhiwen, Li Peijun, Fen Xiqi and Xue Zhilim (China: CAS Shanghai Branch Press) p 167
[5] Weber M J and Monchamp R R 1973 *J. Appl. Phys.* **44** 5495
[6] Korzhik M V, Kudryavtseva A P and Lyubetskii S V 1992 *Zh. Prikl. Spektrosk.* **57** 299
[7] Sakai E 1987 *IEEE Trans. Nucl. Sci.* **34** 418
[8] Holl I, Lorenz E and Mageras G 1987 *IEEE Trans. Nucl. Sci.* **35** 105
[9] Kositin V F, Ragimov T K and Tsumakov A V 1991 *Prib. Tekh. Eksp.* **4** 62
[10] Ryzhikov V D and Sokhin V P 1988 *Instrum. Exp. Tech.* **31** 1303
[11] Bird A J, Carter T, Dean A J, Ramsden D and Swinyard B M 1993 *IEEE Trans. Nucl. Sci.* **40** 395
[12] Brose J, Dahlinger G and Schubert K R 1998 *Nucl. Instrum. Methods Phys. Res.* A **417** 311
[13] Murray R B and Meyer A 1961 *Phys. Rev.* **122** 815
[14] Luntz M 1971 *Phys. Rev.* B **4** 2857
[15] Rodnyi P A, Dorenbos P and van Eijk C W E 1995 *Phys. Status Solidi* b **187** 15
[16] Wojtowicz A J, Glodo J, Wisniewski D and Lempicki A 1997 *J. Lumin.* **72–74** 731
[17] van't Spijker J C, Dorenbos P, van Eijk C W E, Krämer K and Güdel H U 1999 *J. Lumin.* **85** 1
[18] Guilot-Noël O, de Haas J T M, Dorenbos P, van Eijk C W E, Krämer K and Güdel H U 1999 *J. Lumin.* **85** 21
[19] van Loef E V D, Dorenbos P, van Eijk C W E, Krämer K and Güdel H U 2001 *IEEE Trans. Nucl. Sci.* **48** 341
[20] Leverenz H W 1950 An Introduction to luminescence in solids *Structure of Matter Series* ed M G Meyer (London: Wiley) p 270
[21] Rodnyi P A 1992 *Sov. Phys.–Solid State* **34** 1053
[22] Ershov N N, Zakharov N G and Rodnyi P A 1982 *Opt. Spectrosc.* **53** 51
[23] Voloshinovskii A S, Dimitriev A G, Mikhailik V B and Rodnyi P A 1992 *Sov. Phys.–Solid. State* **34** 1998
[24] van't Spijker J C, Dorenbos P, van Eijk C W E, Wickleder M S, Güdel H U and Rodnyi P A 1997 *J. Lumin.* **72–74** 786
[25] Rodnyi P A, Mikhailik V B, Stryganyuk G B, Voloshinovskii A S, van Eijk C W E and Zimmerer G F 2000 *J. Lumin.* **86** 161
[26] Combes C M, Dorenbos P, van Eijk C W E, Krämer K W and Güdel H U 1999 *J. Lumin.* **82** 299
[27] Pawlik Th and Spaeth J-M 1997 *J. Phys.: Condens. Matter* **9** 8737
[28] Mishin A N, Rodnyi P A, Sidorenko A V, Voloshinovskii A S and Dorenbos P 2001 *Proc. SPIE* **4348** 47
[29] Reed J B, Hopkins B S and Audrieth L F 1936 *Inorg. Synth.* **1** 28
[30] Meyer G 1989 *Inorg. Synth.* **25** 146
[31] Zimmerer G 1991 *Nucl. Instrum. Methods* A **308** 178
[32] Moses W W 1993 *A Method to Increase Optical Timing Spectra Measurement Rates Using a Multi-Hit TDC,* Life Sciences Division, Lawrence Berkeley Laboratory, University of California
[33] Rodnyi P A, Mikhrin S B and Mishin A N 2000 *Tech. Phys. Lett.* **26** 678
[34] Dorenbos P, van't Spijker J C, Frijns O W V, van Eijk C W E, Krämer K, Güdel H U and Ellens A 1997 *Nucl. Instrum. Methods Phys. Res.* B **132** 728
[35] van't Spijker J C, de Haas J T M, Dorenbos P, van Eijk C W E, Krämer K W and Güdel H U 1999 *IEEE Trans. Nucl. Sci.* **46** 1274
[36] Dorenbos P 2000 *Phys. Rev.* B **62** 15 650
[37] Voloshinovskii A S, Mikhailik V B, Struk Ya O, Rodnyi P A, van Eijk C W E and Zimmerer G 1998 *J. Lumin.* **79** 115
[38] Mikhailik V B, Voloshinovskii A S, Kisand V and Vielhauer S 1999 *Phys. Status Solidi* b **212** 367

[39] Frisch M J *et al* 1998 *GAUSSIAN98 (REVISION A 1)* (Pittsburgh, PA: Gaussian)
[40] Dorenbos P, Visser R, Dool R, Andriessen J and van Eijk C W E 1992 *J. Phys.: Condens. Matter* **4** 5281
[41] Voloshinovskii A S, Rodnyi P A, Mikhailik V B, Pashuk I P, Antonyak O T and Pidzyrailo M S 1995 *Proc. Int. Conf. on Inorganic Scintillators and their Applications* ed P Dorenbos and C W E van Eijk (Delft: Delft University Press) p 173
[42] Blair I M, Pooley D and Smith D 1972 *J. Phys. C: Solid State Phys.* **5** 1537
[43] Pooley D and Runciman W A 1970 *J. Phys. C: Solid State Phys.* **3** 1815
[44] Tokizaki T, Makimura T, Akiyama H, Nakamura A, Tanimura K and Itoh N 1991 *Phys. Rev. Lett.* **67** 2701
[45] Song K S and Williams R T 1993 *Self-Trapped Excitons (Springer Series on Solid-State Sciences no 105)* ed M Cardona (New York: Springer) p 149
[46] Satpathy S 1986 *Phys. Rev.* B **33** 8706